Decentralized active control of turbulent boundary induced noise and vibration: A numerical investigation

Ming Yuan, Roger Ohayon, Jinhao Qiu

Decentralized active control of turbulent boundary induced noise and vibration: a numerical investigation

Ming Yuan[1], Roger Ohayon[2] and Jinhao Qiu[1]

Noise and vibration induced by turbulent boundary layer (TBL) wall pressure is a widespread issue for aircrafts and vehicles. One way to alleviate this problem is to enhance the structure's sound isolation performance using active structural acoustic control. It is often difficult and costly to generate TBL excitation in laboratories for academic research, especially when the convection velocity is high. Thus, a numerical investigation in the early stages of research is appropriate. This paper proposes a prototyping method. The updated TBL semi-empirical model is chosen through a detailed survey of relevant literature. A tensioned panel used as a control target is intended to simulate realistic aircraft flight conditions. Decentralized control law is considered for active control. A finite element model is built which takes into account the property of TBL excitation. A model reduction technique is also adopted to decrease the order of the analysis model. Numerical simulation results show that the pre-stress effect and the hydrodynamic coincidence have a significant influence on plate vibro-acoustic performance and control channel number selection. Decentralized control of the tensioned plate structure under the pressure of TBL excitation is revealed in this work. A virtual prototyping loop justifies the control law's effectiveness for analyzing TBL excitation. Finally, the procedure proposed may be extended to use in other models or real-life applications.

Keywords
Active noise and vibration control, turbulent excitation, decentralized control, model reduction, numerical simulation

1. Introduction

Turbulent boundary layer (TBL) induced noise and vibration has always been a major concern for the civil aircraft industry. It has attracted increasing academic attention recently, as engine noise, another component of interior noise, has been significantly reduced in the last decades. TBL excitation has the properties of being stochastic and wideband. Generally, an airplane's cruising speed is approximately 0.8 Mach (Wilby, 1996). Therefore, dynamic pressure on the aircraft's skin can be very high, since it is proportional to the square of the free stream velocity. The high levels of noise and vibration that this pressure causes can make passengers uncomfortable and cause structural failure.

Detailed analyses of the turbulent boundary layer theory exist in related literature (Howe, 1998; Schlichting and Gersten, 2000) The large eddy simulation (LES) theory provides a way to simulate turbulence flow (Lesieur, 2005). However, the computational effort involved in using this theory is too intense for a high Reynolds number, and it is difficult to resolve small-scale structures subjected to aerodynamic excitation. Thus, the wall pressure excitation model is usually represented by a semi-empirical spectrum model that is derived from theoretical and experimental results (Blake, 1986).

Simulating the TBL excitation by employing a spectral model has been attempted in the laboratory with an

[1]State Key Laboratory of Mechanics and Control of Mechanical Structures, Nanjing University of Aeronautics and Astronautics, Nanjing, China
[2]Conservatoire National des Arts et Métiers, Structural Mechanics and Coupled Systems Laboratory, Paris, France

Received: 22 December 2013; accepted: 7 December 2014

Corresponding author:
Jinhao Qiu, State Key Laboratory of Mechanics and Control of Mechanical Structures, Nanjing University of Aeronautics and Astronautics, #29 Yudao Street, Nanjing 210016, China.
Email: qiu@nuaa.edu.cn

array of loudspeakers and a discrete implementation (Maury and Bravo, 2006). The main restriction of this method is that unacceptable bias can occur at low speed flows or at high frequencies due to an insufficient number of reproduction sources. Some researchers propose using an analytical method to study aircraft panel vibration and acoustic response under TBL excitation. For instance, the interesting works of Graham (1996), Liu (2008), Efimtsov and Lazarev (2012) cover many aspects of this topic. Other research work (Rocha and Palumbo, 2012) discusses the sensitivities of panel response to spectrum parameters, Mach numbers and correlation-length variations; this work provides valuable analysis of sound radiation and TBL parameters.

On the other hand, to study the exact structure's response under TBL excitation, using a numerical simulation is feasible and convenient for deriving vibroacoustic predictions (De Rosa and Franco, 2008; Ichchou et al., 2009).

Active structure acoustic control is needed to suppress noise and vibration in structures under wide-band excitation, especially at low frequencies. The reason for this is that the passive damping effect of a material is lower at a thickness of less than 1/4 of the disturbance wavelength.

Generally, the active control system is composed of these parts: controller, sensor, actuator and power amplifier. At one time, the active control system suffered from its bulk and complicated electronic system, which restricted its application. Thanks to the development of power electronics and very large scale integration (VLSI) electric technologies, a single active channel today weighs just 60 grams (Schiller et al., 2011). In addition, the field programmable gate array (FPGA) technology has made multi-channel parallel computation possible with very low power consumption (Yuan et al., 2013).

In addition to the hardware, the control algorithm is also pivotal. Many studies have developed various approaches to suppress noise transmission. The feedforward Filtered-x algorithm has been proven suitable for propeller aircraft cabin noise control (Fuller et al., 1997). Some modified methods can increase the Filtered-x algorithm's robustness and performance (Yuan et al., 2012). However, it is difficult to suppress the TBL excitation, which is lowly correlated, using this architecture, and the feedback control architecture is preferred (Rohlfing and Gardonio, 2014). The independent modal space feedback control (IMSC) (Meirovitch, 1990) has been confirmed to be effective for feedback control at very low frequencies. Because a modal filter is needed, the control architecture is generally in multiple input multiple output (MIMO) form. Modal filter implementation also needs careful design. A control observer is usually required when discrete sensors/actuators are available. Another choice is to use distributed sensing, in which sensor layers are trimmed to shape according to specific modal functions. The modal filter determines the number of modes to be controlled. Some researchers use the linear quadratic gaussian (LQG) method to reduce noise (Schiller et al., 2010). As suggested by Doyle et al. (1992), if an observer exists inside the control loop, the stability margin will be arbitrarily small. Robust control (Zhang et al., 2013) improves the system's stability; however, as model-based control, it may suffer from control failure due to temperature and pressure variation. Further, parameters and dynamic uncertainties' influences to the closed loop performance and stability are discussed by the same authors (Zhang et al., 2014). From the energy consumption point of view, four active control laws are studied and compared by Wang and Inman (2011), which is valuable for simultaneously vibration control and energy harvesting.

Concerning the active control of TBL induced noise and vibration, Gibbs et al. (2004) carried out an experimental investigation of test panels at Mach 0.1 and 0.2 conditions. Integrated 10 dB reductions are observed over 150–1000 Hz. However, the proposed generalized predictive control (GPC) control law is still a model based, which needs sophisticated system identification procedure. Control performance and robustness can't be guaranteed if the operating condition is changed. Volume velocity control is also proposed to suppress the first radiation mode of a plate (Maury et al., 2001); however the robustness of the method is not discussed. In addition, the distributed sensing is usually fragile and very expensive.

Contrary to the above-mentioned control laws, collocated direct velocity feedback is considered to be unconditionally stable theoretically (Balas, 1979). The pole-zero interlacing property of collocated configuration guarantees a 90 degrees phase margin (Preumont, 2011). The decentralized sensor/actuator pair is more applicable in aerospace engineering than in other forms mentioned above (Gardonio, 2002). Even if one decentralized control loop fails, another control loop might remain stable. Another advantage of collocated velocity feedback is that it does not require a system-identification process. This advantage is especially useful to control noise and vibration induced by TBL wall pressure. Spillover occurs more easily with the centralized control law. Factors such as robust stability and robust performance must also be subjected to rigorous consideration. Because the centralized control requires precise system modeling and identification, the controller is sensitive to structure variation. Multichannel decentralized control has been analyzed and implemented successfully, providing valuable insights for active sound radiation control and

yielding significant reduction in sound radiation and vibration kinetic power (Gardonio et al., 2004a; Gardonio et al., 2004b; Bianchi et al., 2004; Gardonio and Elliott, 2005b). Centralized (such as LQG control law) and decentralized control performances are demonstrated to be almost equal when the control effort is uniform (Engels et al., 2006).

Although much research exists on structural responses to TBL excitation, and also on active control methods of noise and vibration, the combination of both subjects in one study is rare. The main difficulty lies in the fact that conducting active experiments in a high-speed wind tunnel is complex and costly. A high-speed wind tunnel and a large anechoic chamber are required to conduct the test and evaluate the control effect. On the other hand, in the early stages of research, numerical investigation of the structure's response and active control of its effectiveness under TBL excitation can provide valuable insights. The pioneering research work of Rohlfing and Gardonio (2009) compares deterministic and stochastic excitation for decentralized active control. More detailed discussions may be found in a book chapter they published recently (Gardonio, 2013). However, this work does not consider the structure's tensioned effect under realistic aircraft flight conditions, which this study highlights. This study also finds that volumetric control performance may be limited, and multichannel decentralized control is necessary, for such working conditions. Our numerical results provide valuable insights for low-noise aircraft cabin environmental design. They also show a practical way to combine multiple kinds of subjects into one closed loop; such a concurrent design is very promising in modern aerospace or vehicle engineering.

Section 2 surveys the characteristics of TBL wall pressure and determines which models are most appropriate to use for simulations. Structural vibration under stochastic excitation is also briefly presented. Section 3 presents a two-step model order reduction procedure, which reduces the model while maintaining satisfactory accuracy. Section 4 set up the computation model of a flat panel. Structural mesh and acoustic mesh are thoroughly considered for the TBL excitation and computation band to ensure accurate and compelling computational results. Section 5 provides a detailed discussion of the influence of TBL excitation and the prepress effect on the structure and couplings. Open-loop simulation results indicate that the pressurization effect could change the structure's response dramatically; therefore, non-model based control law is necessary. Satisfying model order reduction within the control band is achieved by using the proposed two-step method. Closed-loop analysis and active control results are further discussed and evaluated in the latter part of this section.

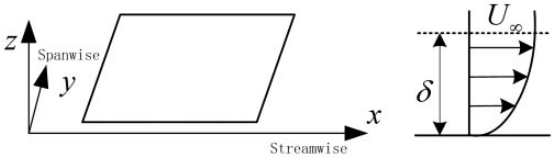

Figure 1. Schematic diagram of the TBL wall pressure excitation.

2. TBL wall pressure model selection and plate response

2.1. Characteristics of the TBL wall pressure

A flat panel with streamwise and spanwise directions is shown in Figure 1. The stream direction is defined along the x axis, and the spanwise direction is defined along the y axis. The turbulent boundary layer is assumed to be fully developed. The boundary layer thickness is defined as δ and the free stream velocity is defined as U_∞. The space-time spectrum model can be decomposed by the multiplication of the auto spectrum density $S_p(\omega)$ and a spatial correlation function $f_c(\xi_1, \xi_1, \omega)$:

$$S_{pp}(\xi_1, \xi_2, \omega) = S_p(\omega) f_c(\xi_1, \xi_1, \omega) \tag{1}$$

where ξ_1, ξ_2 is the separation distance in x axis and y axis respectively.

According to equation (1), the auto spectrum density model and the spatial correlation function are needed to be determined.

2.2. Auto spectral density model and spatial correlation model

A comprehensive review of various TBL wall pressure spectrum models is given by Hwang et al. (2009), in which a set of semi-empirical spectrum models from 1960s to 2004 are compared. These models include Maestrello model, Cockburn-Robertson model, Efimtsov model, Witting model, Chase and Chase-Howe models, Smol'yakov-Tkachenko and Smol'yakov models, and Goody model. As suggested by Huang, the most recent Goody model provides the best agreement with the measured data compared to other models, making it suitable to predict turbulent boundary wall pressure spectrum over wide range Reynolds number. Goody model is actually a modification of Chase-Howe model with many experimental data sets, which may explain its high accuracy. Another review carried out by Miller et al. (2012) compares experimental results with Robertson model, Efimtsov model, Rackl and Weston model, Chase-Howe model,

Goody model, and Smol'yakov model. The conclusion is among these models, Goody model is still the most appropriate single-point wall pressure spectrum model for aircraft applications.

Therefore, it is believed that Goody model is appropriate for our following numerical investigation. The detailed expression of Goody model is defined as (Goody, 2004)

$$S_p(\omega) = \frac{3.0(\delta/U_\infty)^3(\omega\tau_\omega)^2}{[(\omega\delta/U_\infty)^{0.75} + 0.5]^{3.7} + [(1.1R_T^{-0.57})(\omega\delta/U_\infty)]^7} \tag{2}$$

where $R_T = U_\tau^2\delta/U_\infty\upsilon$, with U_τ the friction velocity, δ the boundary layer thickness, U_∞ the freestream velocity, υ the kinematic viscosity, τ_ω the wall shear stress, and ω the angular velocity.

Choosing the spatial correlation wall pressure model is also essential for the accuracy of the velocity prediction, and thus for the accuracy of the sound radiation prediction. The frequently used spatial correlation models are Corcos (1963) model, Efimtsov (1982) model, Chase (1987) model etc.

According to the recent in-flight measurements of jet-powered aircraft by Liu et al. (2012), the Corcos model has been testified to fit the experimental measurements best among the models mentioned above. The Efimstov model and Chase models give underestimated results at the low frequencies, with the Efimtsov model 3–6 dB lower, and the Chase model 1–3 dB lower. The analysis presented by Maury et al. (2002) also suggests that the Corcos model is suitable for high flow aircraft case, whereas the Chase model is appropriate for low flow circumstance. Given the considerations above, the Corcos model is chosen for our simulation.

The Corcos model gives a spatial correlation function formulated as

$$\begin{aligned} f_c(\xi_1, \xi_2, \omega) &= e^{-|\xi_1|/L_1} e^{-|\xi_2|/L_2} e^{-i\omega\xi_1/U_c} \\ &= e^{-\alpha_1\omega|\xi_1|/U_c} e^{-\alpha_2\omega|\xi_2|/U_c} e^{-i\omega\xi_1/U_c} \end{aligned} \tag{3}$$

The correlated value is supposed to decay exponentially with distance.

The coherence length in streamwise (L_1) is defined as $L_1 = \frac{U_c}{\alpha_1\omega}$, and the coherence length in spanwise (L_2) as $L_2 = \frac{U_c}{\alpha_2\omega}$. U_c is the convective velocity. Parameters of α_1 and α_2 are generally chosen in the literature as $\alpha_1 = 0.10$ and $\alpha_2 = 0.77$.

2.3. Structure responses under random excitation

The finite element model of the structure can be discretized into n degrees of freedom. The $n \times n$ dimension matrix of mass, damping and stiffness are [**M**], [**C**] and [**K**] respectively. The damping matrix is assumed to be frequency independent.

The $n \times n$ dimension of transfer function matrix which links displacement and force is defined as

$$[\mathbf{H}(\omega)] = \left[-\omega^2\mathbf{M} + j\omega\mathbf{C} + \mathbf{K}\right]^{-1} \tag{4}$$

In physical domain, spectrum density relation of excitation and response has the form of (Ohayon and Soize, 2014)

$$[\mathbf{S}_X(\omega)] = [\mathbf{H}(\omega)][\mathbf{S}_F(\omega)][\mathbf{H}^*(\omega)]^T \tag{5}$$

where the $n \times n$ dimension matrix $[\mathbf{S}_X(\omega)]$ is cross spectrum density of displacement response, the $n \times n$ dimension matrix $[\mathbf{S}_F(\omega)]$ is cross spectrum density of excitation force, $[\mathbf{H}^*(\omega)]$ is the conjugate form of matrix $[\mathbf{H}(\omega)]$ the star $*$ denotes complex conjugate and the dimension is $n \times n$.

The corresponding velocity spectral matrix can also be derived as

$$\left[\mathbf{S}_{\dot{X}}(\omega)\right] = \omega^2[\mathbf{H}(\omega)][\mathbf{S}_F(\omega)][\mathbf{H}^*(\omega)]^T \tag{6}$$

When the sound radiation is considered, the sound pressure should satisfy the Helmholtz equation

$$\nabla^2 p + k^2 p = 0 \tag{7}$$

where $k = \omega/c$ is the acoustic wavenumber.

At the excitation surface, the boundary condition is

$$\nabla p \cdot \mathbf{n} = -\rho a_n \tag{8}$$

where $\mathbf{n}$ is the unit vector normal to the radiating surface and a_n the acceleration normal to the radiation surface.

At the infinite domain, the sound radiation problem should satisfy the Sommerfeld condition (Ohayon and Soize, 1998)

$$\lim_{r\to\infty} r\left(\frac{\partial p}{\partial r} + jkp\right) = 0 \tag{9}$$

3. Model order reduction and active control law design

3.1. Model order reduction

As indicated in the introduction section, collocated decentralized velocity feedback control is adopted for the following analysis, and each control loop is SISO form. However, when finite element method (FEM) results are utilized to derive the transfer function

without any reduction, the model order can be as high as thousands of orders. Such bulky matrix makes analysis and simulation in control domain almost impossible. Luckily, modal representation could downscale the FEM model to a large extent, since the admittance of selected position in physical domain can be represented by selected row/column from the computed modal matrix.

For the modal damping case, the generalized damping matrix can be diagonalized as: $C = \mathbf{\Phi}^T \mathbf{C} \mathbf{\Phi} = diag(2\zeta_r \omega_r M_r)$. $\mathbf{\Phi} = [\phi_1\ \phi_2\ \cdots\ \phi_N]$ is the modal matrix whose columns are the respective normal modes. The N uncoupled equation of motion in modal domain will have the form as

$$M_r \ddot{\eta}_r + 2M_r \omega_r \zeta_r \dot{\eta}_r + \omega_r^2 M_r \eta_r = \phi_r^T \mathbf{p}(t), \quad r = 1, 2, \ldots, N \tag{10}$$

If the modal mass is normalized to unity, then for one specific mode, the modal equation is

$$\ddot{\eta}_r + 2\xi_r \omega_r \dot{\eta}_r + \omega_r^2 \eta_r = f_r(t) \quad r = 1, 2, \ldots, N \tag{11}$$

When the modal displacement η_r and the modal velocity $\dot{\eta}_r$ are chosen to be state variables, the state space form can be expressed as follows

$$\begin{bmatrix} \dot{\eta}_r \\ \ddot{\eta}_r \end{bmatrix} = \begin{bmatrix} 0 & 1 \\ -\omega_r^2 & -2\xi_r \omega_r \end{bmatrix} \begin{bmatrix} \eta_r \\ \dot{\eta}_r \end{bmatrix} + \begin{bmatrix} 0 \\ f_r \end{bmatrix} u \tag{12}$$

The system matrix is

$$\mathbf{A} = \begin{bmatrix} 0 & 1 \\ -\omega_r^2 & -2\xi_r \omega_r \end{bmatrix}$$

and the input matrix is $\mathbf{B} = \begin{bmatrix} 0 \\ f_r \end{bmatrix}$. When the output is modal displacement, the $\mathbf{C}$ matrix is $\begin{bmatrix} 1 & 0 \end{bmatrix}$. When the output is modal velocity, the $\mathbf{C}$ matrix will be $\begin{bmatrix} 0 & 1 \end{bmatrix}$. The matrix of $\mathbf{D}$ is zero under this circumstance.

Supposing the upper analysis circular frequency is specified to be ω_a, to minimize the influence of residue modes, the highest natural circular frequency ω_{up} obtained by modal analysis should be no less than $3\omega_a - 5\omega_a$.

After the analysis band is determined, the global state space model in the modal domain has the form of

$$\begin{bmatrix} \dot{\eta}_1 \\ \ddot{\eta}_1 \\ \vdots \\ \vdots \\ \dot{\eta}_{up} \\ \ddot{\eta}_{up} \end{bmatrix} = \begin{bmatrix} 0 & 1 & 0 & 0 & \cdots & \cdots \\ -\omega_1^2 & -2\xi_1\omega_1 & 0 & 0 & \cdots & \cdots \\ \cdots & \cdots & \cdots & \cdots & \cdots & \cdots \\ \cdots & \cdots & \cdots & \cdots & \cdots & \cdots \\ 0 & 0 & \cdots & \cdots & 0 & 1 \\ 0 & 0 & \cdots & \cdots & -\omega_{up}^2 & -2\xi_{up}\omega_{up} \end{bmatrix} \times \begin{bmatrix} \eta_1 \\ \dot{\eta}_1 \\ \vdots \\ \vdots \\ \eta_{up} \\ \dot{\eta}_{up} \end{bmatrix} + \begin{bmatrix} 0 \\ f_1 \\ \vdots \\ \vdots \\ 0 \\ f_{up} \end{bmatrix} u \tag{13}$$

Accordingly, when the physical representation is transformed into modal domain, the order of the state space model is greatly reduced from $2n$ to $2n_{up}$, with n the degrees of system of the original system and n_{up} the modal order determined by ω_{up}.

Remark: In vibro-acoustic analysis, usually only the degrees of system in the vertical direction of plate structure are considered. Hence, the analyzed number of degrees of system equals to the meshed structure which has n node numbers.

After this step, the order of the state space equation in modal domain could still be as high as hundreds for wide band consideration. Therefore, it is desirable to reduce the model order further on the transfer function. Two simple and computation inexpensive model reduction methods are illustrated as follows (Skogestad and Postlethwaite, 1996).

Assuming the original state space system representation $(\mathbf{A}, \mathbf{B}, \mathbf{C}, \mathbf{D})$, after appropriate manipulation, can be expressed as

$$\begin{aligned} \dot{\mathbf{x}}_1 &= \mathbf{A}_{11}\mathbf{x}_1 + \mathbf{A}_{12}\mathbf{x}_2 + \mathbf{B}_1\mathbf{u} \\ \dot{\mathbf{x}}_2 &= \mathbf{A}_{21}\mathbf{x}_1 + \mathbf{A}_{22}\mathbf{x}_2 + \mathbf{B}_2\mathbf{u} \\ \mathbf{y} &= \mathbf{C}_1\mathbf{x}_1 + \mathbf{C}_2\mathbf{x}_2 + \mathbf{D}\mathbf{u} \end{aligned} \tag{14}$$

$\dot{\mathbf{x}}_2$ is the state vector to be removed. The first model reduction method is through residualization. For the SISO form which will be used for decentralized control, the reduced form is

$$\begin{aligned} \dot{\mathbf{x}}_1 &= \mathbf{A}_r\mathbf{x}_1 + \mathbf{B}_r u \\ y &= \mathbf{C}_r\mathbf{x}_1 + \mathbf{D}_r u \end{aligned} \tag{15}$$

where $\mathbf{A}_r = \mathbf{A}_{11} - \mathbf{A}_{12}\mathbf{A}_{22}^{-1}\mathbf{A}_{21}$, $\mathbf{B}_r = \mathbf{B}_1 - \mathbf{A}_{12}\mathbf{A}_{22}^{-1}\mathbf{B}_2$, $\mathbf{C}_r = \mathbf{C}_1 - \mathbf{C}_2\mathbf{A}_{22}^{-1}\mathbf{B}_2$, $\mathbf{D}_r = \mathbf{D} - \mathbf{C}_2\mathbf{A}_{22}^{-1}\mathbf{B}_2$. The matrix of $\mathbf{A}_{22}$ is supposed to be invertible. The new system of $(\mathbf{A}_r, \mathbf{B}_r, \mathbf{C}_r, \mathbf{D}_r)$ is called the residualization of the original system.

The residualizing method has the advantage of preserving the output steady state gain. However, the high frequency response is biased and the reduced model

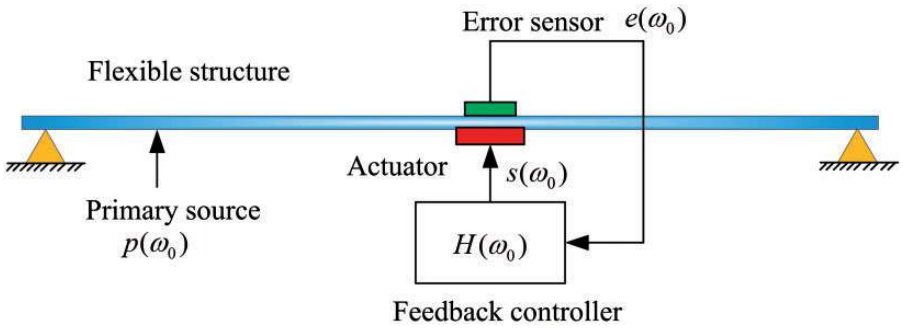

Figure 2. Collocated direct velocity feedback control.

contains a non-zero direct feed-through matrix $\mathbf{D}_r$, which is usually undesirable.

The second method is modal truncation. Physical interpretation can be easily retained using this method, and the high frequency response trend is close to the real system. However, the steady state gain is not the same as the original value. Some important modes at high frequencies may be discarded inappositely and the global accuracy is not satisfying.

In order to present a more accurate model with a wide frequency range, errors at the low frequency and the high frequency should be both considered. The modal information can be computed by fast and reliable FEM solver. Since each mode plays a different role for the frequency response, the next step is to sort from high to low the contribution of the modes before modal truncation.

The collocated transfer function is made up by the mode's combination as

$$\frac{x_k}{F_k} = \sum_{i=1}^{n_r} \frac{\phi_{ki}\phi_{ki}}{s^2 + 2\xi_i\omega_i s + \omega_i^2} \tag{16}$$

Consider the static gain of each mode, which can be simply expressed as

$$G_{static} = \frac{\phi_{ki}\phi_{ki}}{\omega_i^2} \tag{17}$$

At the resonance frequency, the vibration amplitude of each mode is also linked by the G_{static}

$$G_{resonance} = \frac{\phi_{ki}\phi_{ki}}{j2\xi_i\omega_i^2} = \frac{1}{j2\xi_i} G_{static} \tag{18}$$

Therefore, the parameter of G_{static} plays an important role in the structure's response. After reordering, modes that have lower contributions to the frequency response can be discarded. Due to crucial information has been preserved, compared to the original system, this reduction has only tiny influences on the system's steady and the dynamic property.

3.2. Active control law design

As shown in section 5, the atmosphere parameters could change the panel's modal frequencies a lot, the structure to be controlled can be treated as a time-varying system (as the altitude of aircraft can be changed, the atmosphere parameters will be also changed), the non-model based control law is suitable under this circumstance. Here, collocated direct velocity feedback control is selected to generate active damping on the structure, as shown by the schematic diagram in Figure 2.

When actuators generate control force on the structure, the modal equation is

$$\mathbf{I}\ddot{\eta} + diag(2\omega_1\zeta_1, 2\omega_2\zeta_2, \cdots 2\omega_n\zeta_n)\dot{\eta} + diag(\omega_1^2, \omega_1^2, \cdots \omega_n^2)\eta = \mathbf{\Phi}^T\mathbf{B}\mathbf{u} \tag{19}$$

$\mathbf{u}$ is the control signal vector with a dimension of $m \times 1$. $\mathbf{B}$ is the input influence matrix of dimension $n \times m$. For collocated feedback, the output velocity from the sensor signal is

$$\dot{\mathbf{y}} = \mathbf{B}^T\dot{\mathbf{x}} \tag{20}$$

And the control signal $\mathbf{u}$ is

$$\mathbf{u} = -\mathbf{G}\dot{\mathbf{y}} = -\mathbf{G}\mathbf{B}^T\mathbf{\Phi}\dot{\eta} \tag{21}$$

where $\mathbf{G}$ is the gain matrix.

After some manipulation, the final dynamic equation can be written as

$$\mathbf{I}\ddot{\eta} + (diag(2\omega_1\zeta_1, 2\omega_2\zeta_2, \cdots 2\omega_{up}\zeta_{up}) + \mathbf{\Phi}^T\mathbf{B}\mathbf{G}\mathbf{B}^T\mathbf{\Phi})\dot{\eta} + diag(\omega_1^2, \omega_1^2, \cdots \omega_n^2)\eta = \mathbf{0} \tag{22}$$

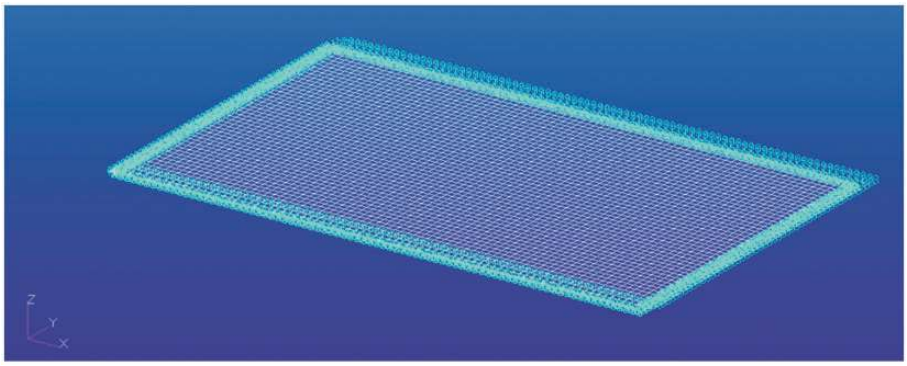

Figure 3. Plate with simple supported boundary condition.

For decentralized control, the gain matrix $\mathbf{G}$ is diagonal. For small gains, the matrix of $\mathbf{\Phi}^T\mathbf{B}\mathbf{G}\mathbf{B}^T\mathbf{\Phi}$ can be considered as diagonally dominant (Preumont, 2011), and the decoupled equation could be obtained.

For the i-th mode, the modal equation is

$$\ddot{\eta}_i + (2\omega_i\zeta_i + g)\dot{\eta}_i + \omega_i^2\eta_i = 0 \tag{23}$$

therefore active damping is achieved. The mechanism of active damping control determines this control strategy is mainly effective in the vicinity of the vibration resonances. If the structure has been well damped, this method will not be advisable.

The final control result depends closely on the sensor/actuator number and location, as sensor can only detect local vibration information of the structure. Thus, it is inevitable that the sensor/actuator pair localizes on nodal lines for some modes. These modes are neither controllable nor observable.

4. Computation setup

As showed in Figure 3, the computation model is a simple supported flat plate. The curvature is removed since the fuselage's dimension is much larger compared to the bay's. The modal damping ratio is set to be 0.01 for all frequencies, and the plate vibration can be treated independently above 500 Hz since the correlation is low with adjacent panels (Maury et al., 2002).

The physical parameters of the panel are given in Table 1. They are chosen to be close to bay parameters of the ARJ-21 jet aircraft.

The turbulent boundary parameters for the Goody's model are given in Table 2. The corresponding values are validated at the cruise state for jet airplane. Related atmosphere parameters can be calculated according to the US Standard Atmosphere 1976.

As the internal pressure exists inside the cabin when the airplane flies, longitudinal stress and hoop stress generate a tensioned effect on the plate. The longitudinal tension force is assumed to be 29.3×10^3 N/m and the hoop tension force is assumed to be 62.1×10^3 N/m (Graham, 1996).

Table 1. Physical parameters of the panel.

Parameters	Corresponding values
Length	0.4 m
Width	0.245 m
Thickness	0.001 m
Material	Aluminum
Young's Modulus	72 GPa
Density	2800 kg/m^3
Poisson's ratio	0.33

Table 2. Parameters for the TBL wall pressure models.

Parameters	Values
Atmosphere density	0.44 kg/m^3
Sound speed	300 m/s
Free stream velocity	240 m/s
Friction velocity	6.75 m/s
Boundary layer thickness	0.08 m
Kinematic viscocity	3.3553×10^{-5}
Covective velocity	168 m/s
Corcos model of α_1	0.10
Corcos model of α_2	0.77

The mesh size is mainly determined by two key issues. Firstly, the bending wavelength at the highest analysis frequency should comprise at least 6 elements. The wavelength value of a plate structure is

$$\lambda(\omega) = 2\pi\left(\frac{Eh^2}{12\rho\omega^2(1-\upsilon^2)}\right)^{1/4} \tag{24}$$

where ρ is the material density, h the plate thickness, E the Young's modulus, and υ the Poisson's ratio.

When the analysis band between 10 Hz and 3.5 kHz, if the modal frequency response method is used, the upper modal frequency is set to be 24 kHz, which is almost seven times of the upper frequency for sound power calculation.

Secondly, the turbulent wavelength should also be considered. The associated wavelength with respect to convective velocity is

$$\lambda = \frac{U_c}{f} \tag{25}$$

In our case, $\lambda = 168/3500 = 0.048$ m. The wavelength should also comprise 6 elements, thus the mesh edge length should be no larger than 0.008 m.

Combining the above two criteria, in this simulation, the mesh size scales on the flexural is much finer than the mesh size scales on the convective wavelength. Thus, the mesh size is scaled on the flexural. The final size of structure mesh is set to be 0.003 m. The modal results are computed by using MSC. Nastran©.

For the acoustic domain, the acoustic wavelength can be computed according to

$$\lambda_{acoustic} = \frac{c}{f_{cutoff}} \tag{26}$$

The final size of acoustic finite element mesh is set to be 0.01 m.

The sound radiation of the panel is computed using a finite/infinite element approach, which is integrated in MSC.Actran©. The infinite elements behave as non reflective boundary condition (NRBC), which satisfy the Sommerfeld condition. Besides the infinite elements, the acoustic finite elements should also be created near the radiating structure, which could capture the near-field sound characteristics and help getting accurate far field acoustic responses. Virtual microphones are added as field points to obtain radiated sound power according to the ISO 3744 standard. The solver type is 'MUMPS'(a MUltifrontal Massively Parallel sparse direct Solver), and the final model is shown in Figure 4.

5. Simulation results

5.1. Tensioned and un-tensioned vibro-acoustic responses comparison

The first nine mode shapes and natural frequencies of the un-tensioned plate are summarized in Figure 5 and the tensioned case results are shown in Figure 6. Since the plate is simply supported, the modal frequency with different mode numbers can also be calculated analytically. The simulation results are verified to be highly consistent with the analytical cases.

As stated in section 4, the fuselage bay behaves like vibrating independently above 500 Hz. Due to the in-plane tension force, here, only two modes (339.04 Hz and 415.87 Hz) are below 500 Hz. As a consequence, the main characteristic of the simplified model is retained.

For wider frequencies, Figures 7 and 8 show the plate's vibration kinetic response and acoustic sound power radiation respectively. The wall pressure excitation is a combination of Goody model and Corcos model, which is determined in section 2.

Figures 7 and 8 show clearly that the panel's vibration and sound radiation power cannot be treated equally. According to the radiation efficiency theory (Wallace, 1972), some selected modes' sound radiation efficiencies are plotted in Figure 9.

For the un-tensioned case, as the odd-odd modes suffer the least acoustic cancellation, thus they have the highest radiation efficiencies. The first vibration mode radiates the most; in consequence, significant global sound radiation suppression can be achieved if this mode is well suppressed. The even-even modes suffer the acoustic cancellation most and have the lowest sound radiation efficiencies. The odd-even and even-odd modes' sound radiation efficiencies are in-between.

When the plate is tensioned, all the natural frequencies move to higher frequencies band compared to the un-tensioned case. For instance, the 1st mode is now 339.04 Hz, which is much larger than the un-tensioned case (55.39 Hz). Besides, the odd-even modes, even-odd modes and even-even modes become more sound radiation effective for the tensioned case. The reason is that, when the natural frequencies move to higher band, the modes' radiation efficiencies will also rise. The acoustic cancellation for the odd-even, even-odd and even-even modes is weakened compared to the low frequencies.

Another property for the structure under TBL excitation is that more modes can make a notable contribution to sound radiation compared to the structure under diffuse excitation. Two different excitation simulation results are given in Figure 10.

One explication is that the diffuse pressure field is actually composed by infinite uncorrelated plane waves from any direction rather than by local stochastic wall pressure. Another notable feature of the TBL excitation is that it couples to the structure unevenly over the frequencies (Gardonio, 2013), due to the hydrodynamic coincidence phenomenon (Graham, 1997).

At such critical frequencies, the convective wavenumber $k_c = \omega/U_c$ and the structure modal wavenumber in direction of the streamwise $k_m = m\pi/a$ are equal. The streamwise length is a and the mode order in this

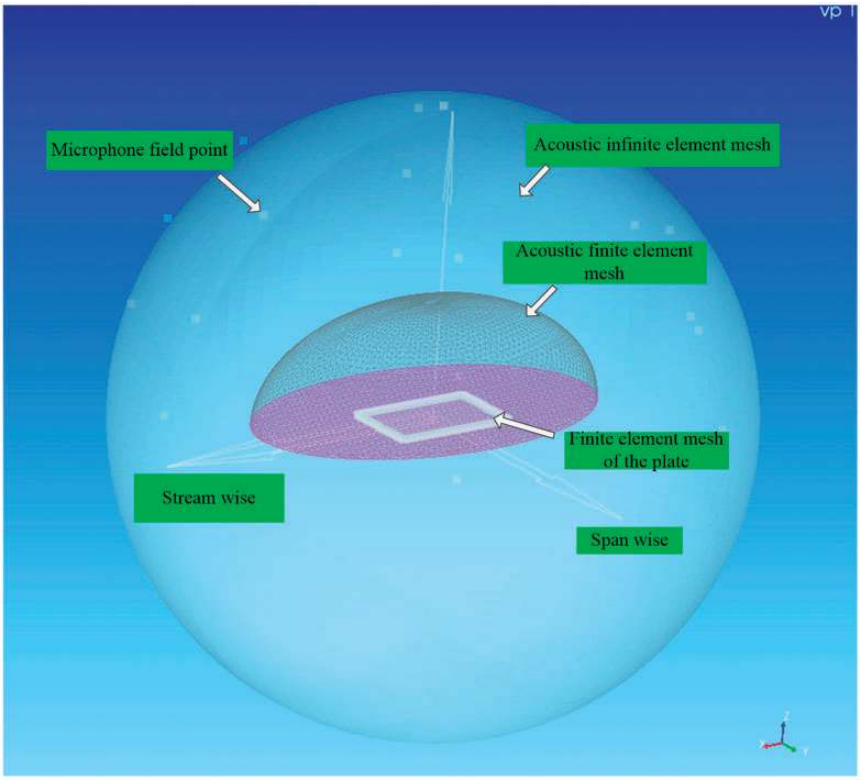

Figure 4. Computation model using finite/infinite element methods.

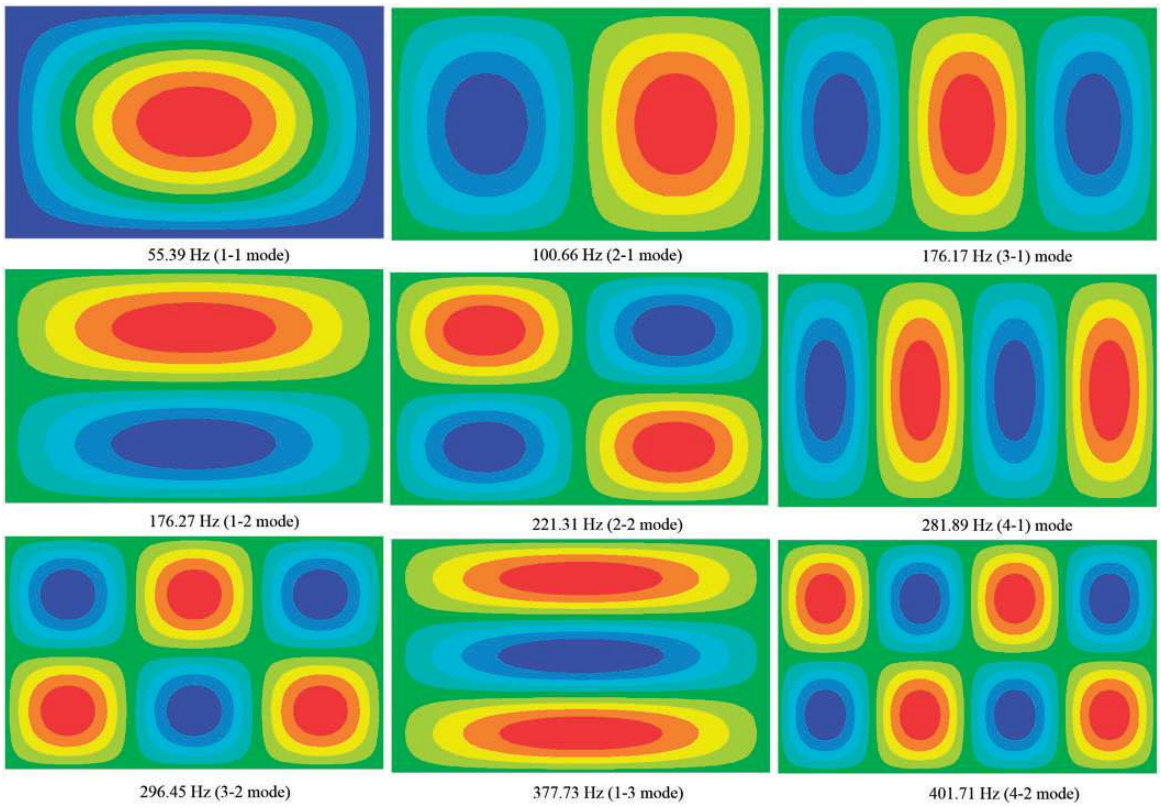

Figure 5. Mode shapes and natural frequencies of the un-tensioned plate.

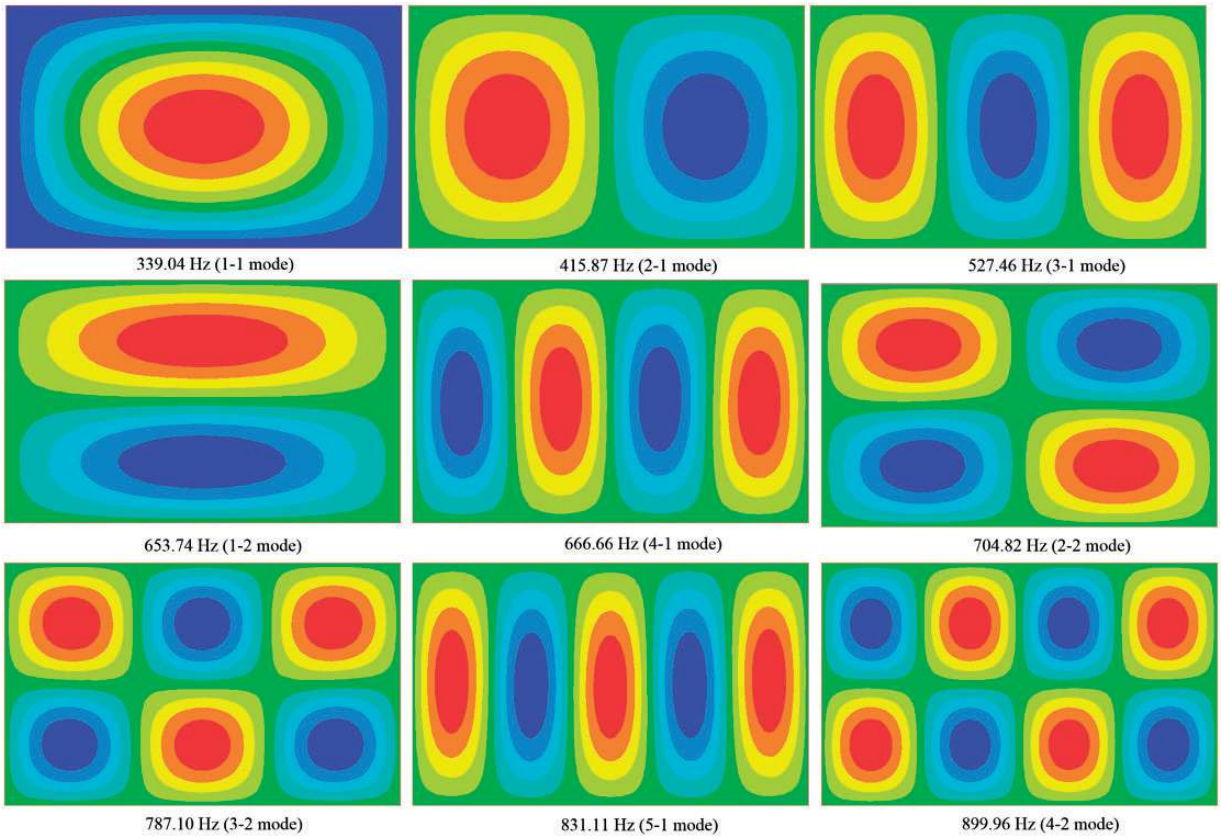

Figure 6. Mode shapes and natural frequencies of the tensioned plate.

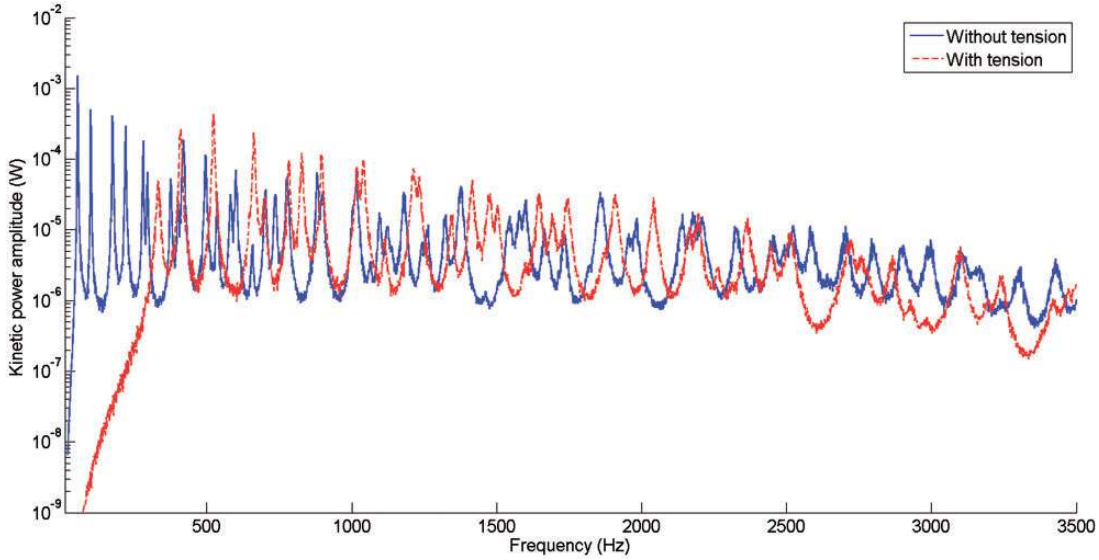

Figure 7. Kinetic power of the plate under TBL excitation (solid line: without tension, dashed line: with tension).

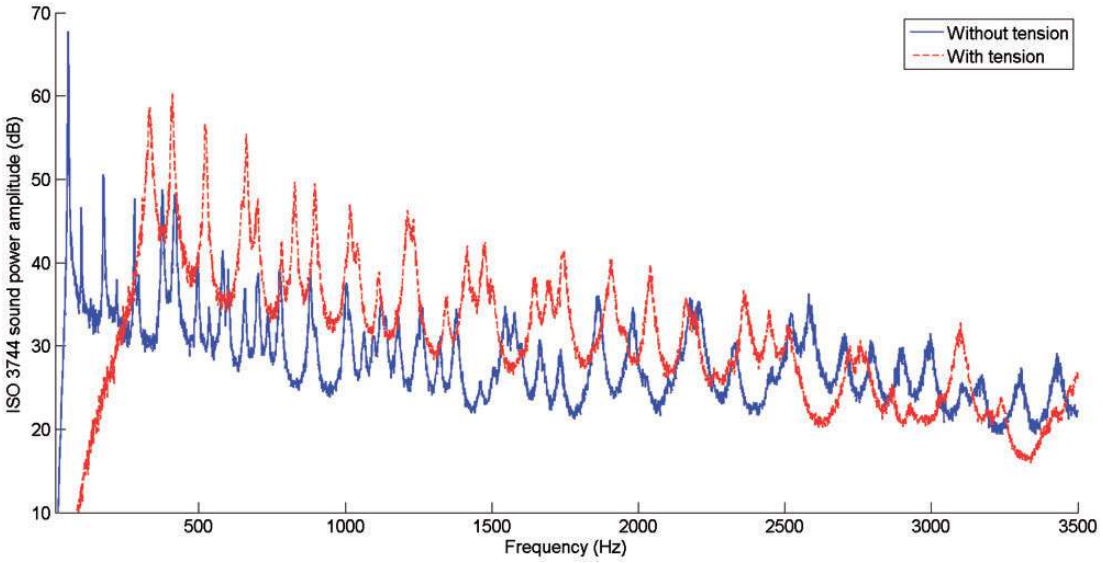

Figure 8. Sound radiation of the tensioned plate under TBL excitation (solid line: without tension, dashed line: with tension).

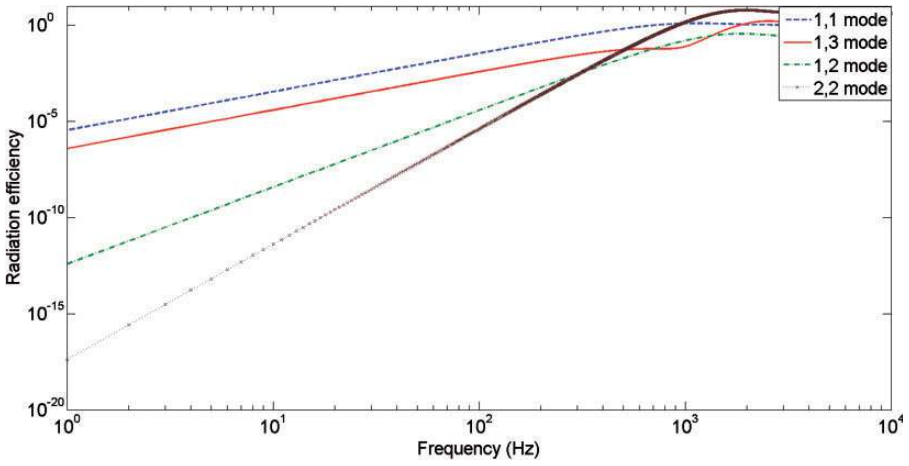

Figure 9. Radiation efficiencies of the panel's selected modes.

direction is m. Therefore, the TBL disturbance can excite the structure neighboring modes easily around convective critical frequencies. In our simulation case, the relationship of streamwise mode number and the convective critical frequencies locations are plotted in Figure 11 (without tension effect) and Figure 12 (with tension effect) respectively.

As shown in Figures 11 and 12, the convective coincidence phenomenon can occur over large frequency range in the analysis band. Accordingly, some acoustic inefficient modes can become strong radiators since they are highly excited. For the tensioned case, this phenomenon will be more severe when the natural frequencies are higher, as the sound radiation efficiencies are increased.

These simulation results indicate that, for the untensioned case, when only the first mode is anticipated to be well suppressed, the sound isolation effect can be prominent. However, for the tensioned case, if only one control pair is used, mainly to suppress the first mode, the sound isolation performance is not satisfying, since other modes (such as 2-1 mode) also contribute significantly to the far field sound radiation. More control pairs are needed under a decentralized architecture.

It also should be mentioned that when the frequency becomes higher, the ridges of the vibro-acoustic

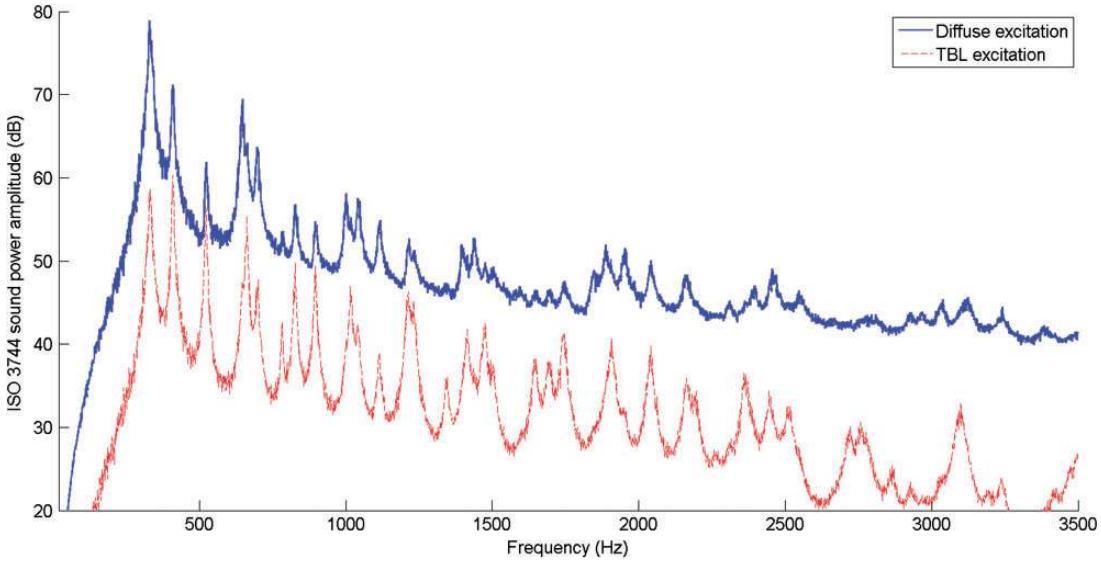

Figure 10. Sound radiation of the tensioned plate according to ISO3744 standard under TBL and diffuse excitation.

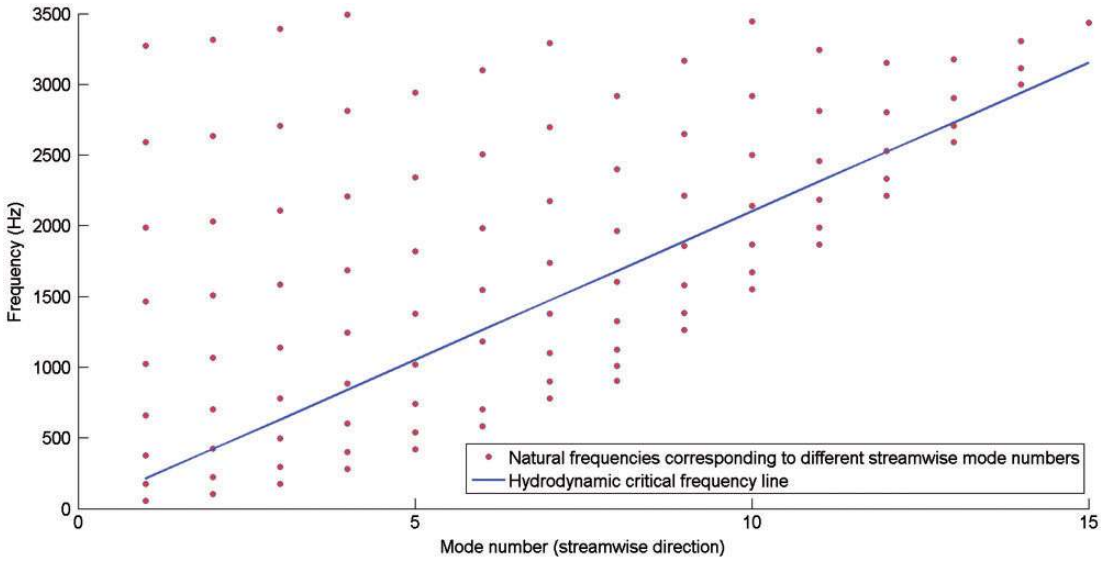

Figure 11. Convective critical frequencies and resonance frequencies of the structure (without tension effect).

response are much wider than the low frequency's response. This is because the modal overlap is more severe than the low frequencies, and the ridge is actually contributed by multiple nearby modes. Therefore, if only some local modes are damped by active control at high frequencies, the global performance may not be satisfying. In addition, for practical implementation of active control system, the latency in the control loop could bring severe phase lag when the frequency is high. Consequently, the control law's frequency response should gradually roll off to guarantee enough gain margin. Based on the above reasons, the following active control band is limited to 1 kHz but the global vibro-acoustic evaluation is extended to 3.5 kHz.

5.2. Model order reduction results

The Nastran© f06 file which contains the modal information is read into MATLAB© for model order reduction and state space matrix generation. Ninety modes

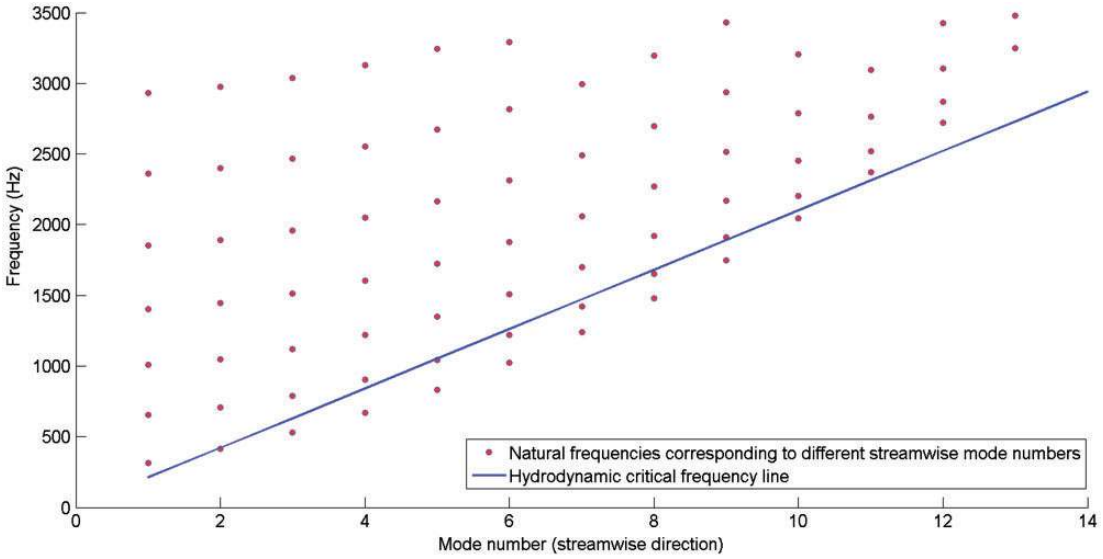

Figure 12. Convective critical frequencies and resonance frequencies of the structure (with tension effect).

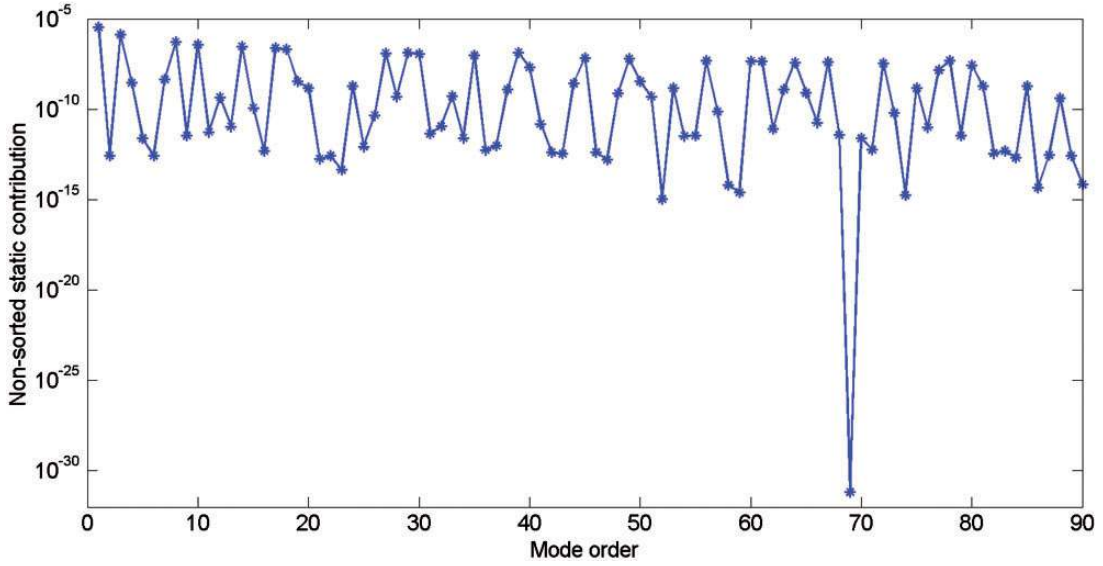

Figure 13. Non-sorted static contribution of each mode.

which cover the frequency band up to 4 kHz are used. When the feedback gain is very high, the panel can be treated as pinned at the control position (Gardonio and Elliott, 2005a; Elliott et al., 2002). This condition can also generate new vibration modes at high frequencies, and more modes are needed correspondingly for this circumstance. Here, since moderate control gain is only considered and no pinning phenomenon will occur, a relatively small number of modes are used.

Consider one sensing point which is located on the middle location of the plate. The non-sorted static contribution of each mode is given in Figure 13 and sorted static contribution of each mode is given in Figure 14.

It can be observed that a few modes make a major contribution to the structure static gain. Thus, it is suggested that only those modes are important for dynamic analysis within the interested band. A judging rule is assumed the reduced order model should generate less than 5% static error compared to the full order

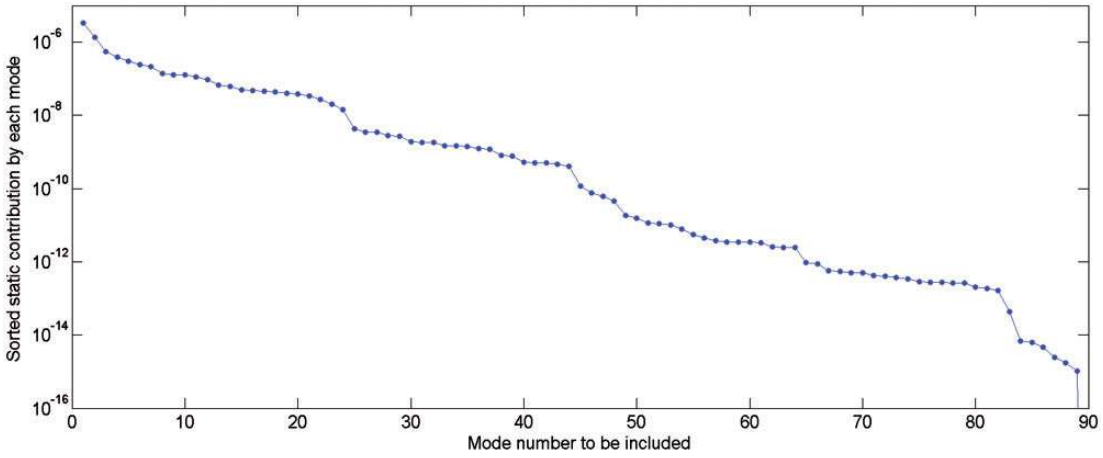

Figure 14. Sorted static contribution of each mode.

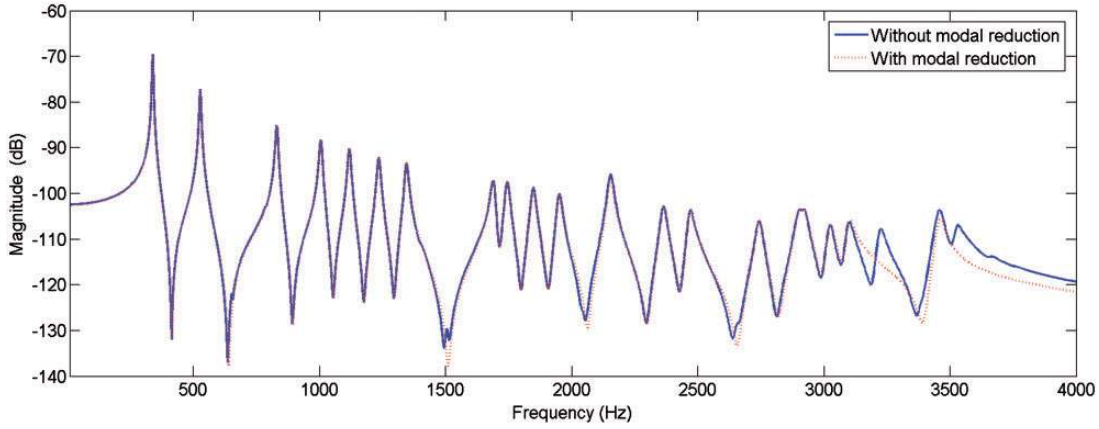

Figure 15. Magnitude responses with only 20 modes included and with 90 modes included.

model. According to this guide, the modal order is set to 20, which could greatly reduce the model size.

Collocated displacement response comparisons with and without modal reduction are given in Figures 15 and 16.

As the selected sensor/actuator locates on the middle of the plate, the 2-1 (415.87 Hz) and 1-2 (653.47 Hz) modes, for instance, are not controllable and observable. Their modal information cannot be seen in the above two figures. This indicates that more actuators should be used for the targeting modes.

5.3. Active control results evaluation

As shown in Figure 8, 1-1, 2-1, 3-1 and 1-2 modes radiate the most under the tensioned circumstance, thus they need to be suppressed. The intended sensor/actuator pair locations are illustrated in Figure 17.

5.3.1. Case 1: with one control pair. Consider the actuator/sensor to be located on the middle point of the tensioned plate (sensor/actuator pair No.1). The corresponding root-locus plot of the SISO velocity feedback control system is given in Figure 18.

Damping information and relevant gain information can be found through this root-locus plot. The optimal gain is obtained when the maximum damping ratio is achieved for the target mode.

Since 1-1 mode is the target mode in this case, the optimal gain is set to be 52. And the maximum damping ratio for the 1st mode is 0.140. This sensor/actuator location can also be used to suppress 3-1 mode and 5-1 mode, where the active damping ratio of 3-1 mode is

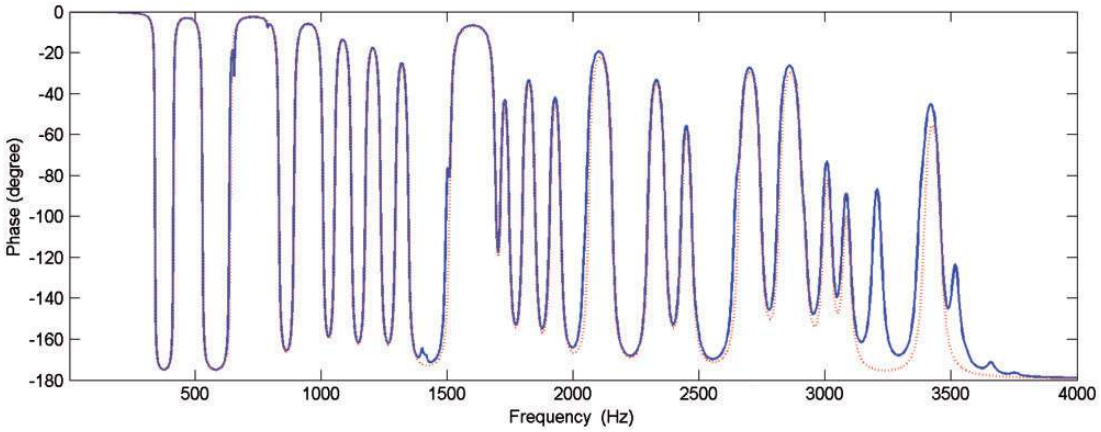

Figure 16. Phase responses with only 20 modes included and with 90 modes included.

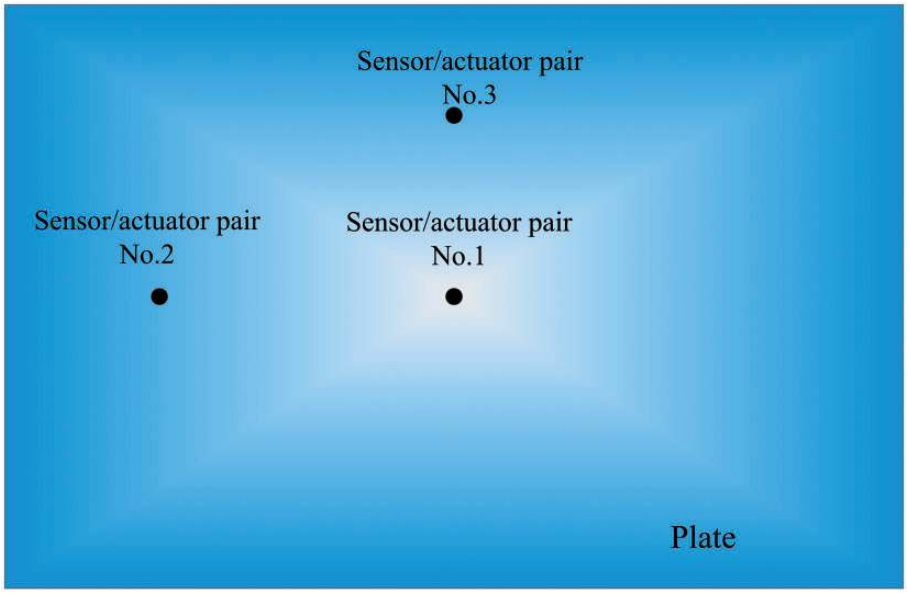

Figure 17. Collocated pairs configuration for decentralized control.

0.142 and 5-1 mode is 0.056 under this gain. Global sound power (10 Hz- 3500 Hz) without control is 75.8 dB. With active control, the global sound power for the frequency band can be lowered by 2.34 dB.

5.3.2. Case 2: with two control pairs. The second actuator is located on the left of the plate (sensor/actuator pair No.2). It is primarily used to suppress the 2-1 mode. Simulation results show that the maximum active damping for this mode is 0.2. The global sound power can be lowered by 4.2 dB for the frequency band below 3.5 kHz for this case.

5.3.3. Case 3: with three control pairs. The third control pair (sensor/actuator pair No.3) is mainly used to control the 1-2 mode, where the maximum active damping is 0.063 with an optimal gain of 35.6. The 3-2 mode can also be suppressed for this control pair location, the damping ratio is 0.115 with the same gain. As more control pairs are adopted, the vibration and sound radiation control results become more prominent. In this case, when three actuators are adopted, the acoustic sound power can be suppressed by 4.9 dB globally.

For different cases, the vibro-acoustic control results are summarized in Figures 19 and 20. Above 1 kHz, the

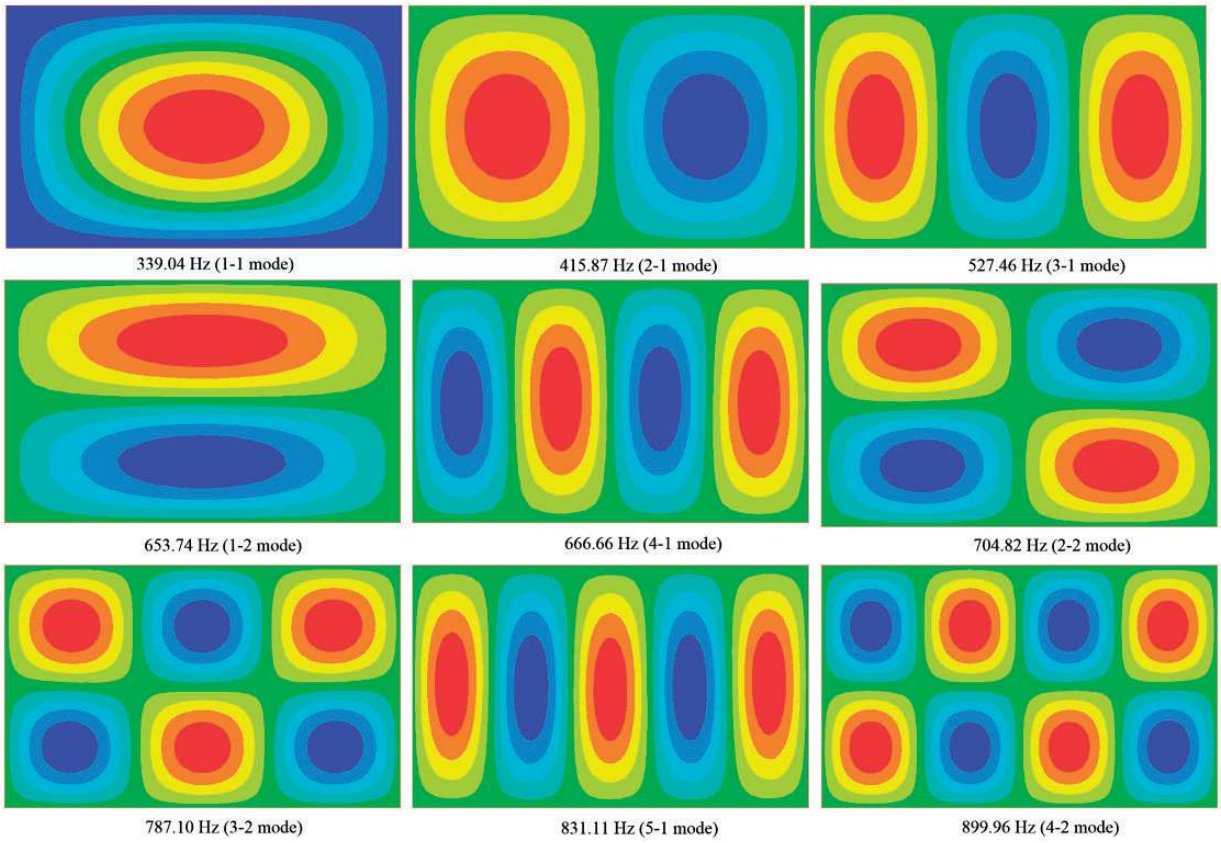

Figure 18. Root-locus plot for the collocated control pair.

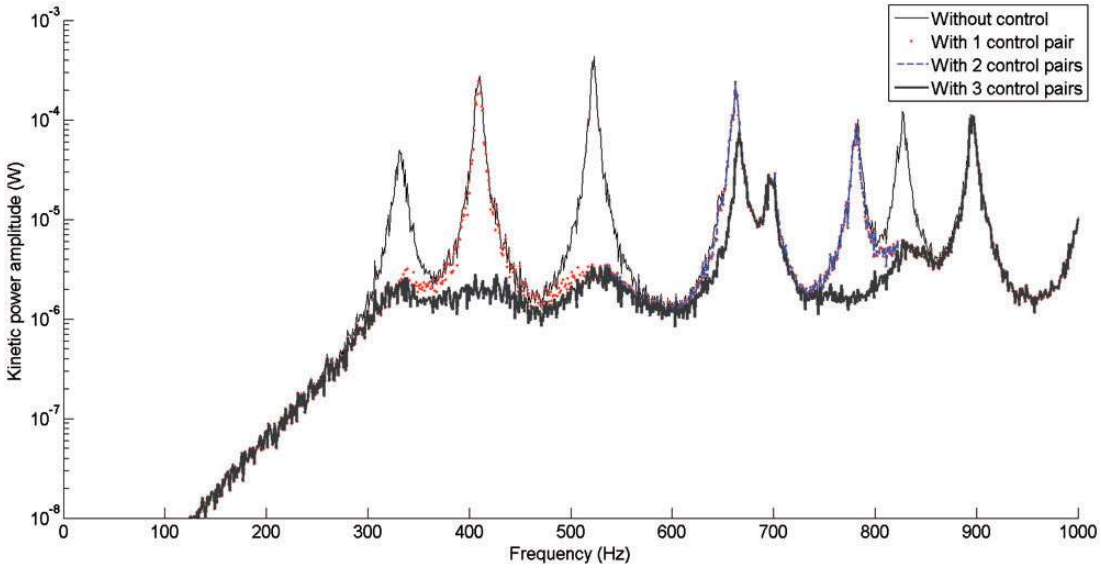

Figure 19. Control result of kinematic power of the plate with different number of control pairs.

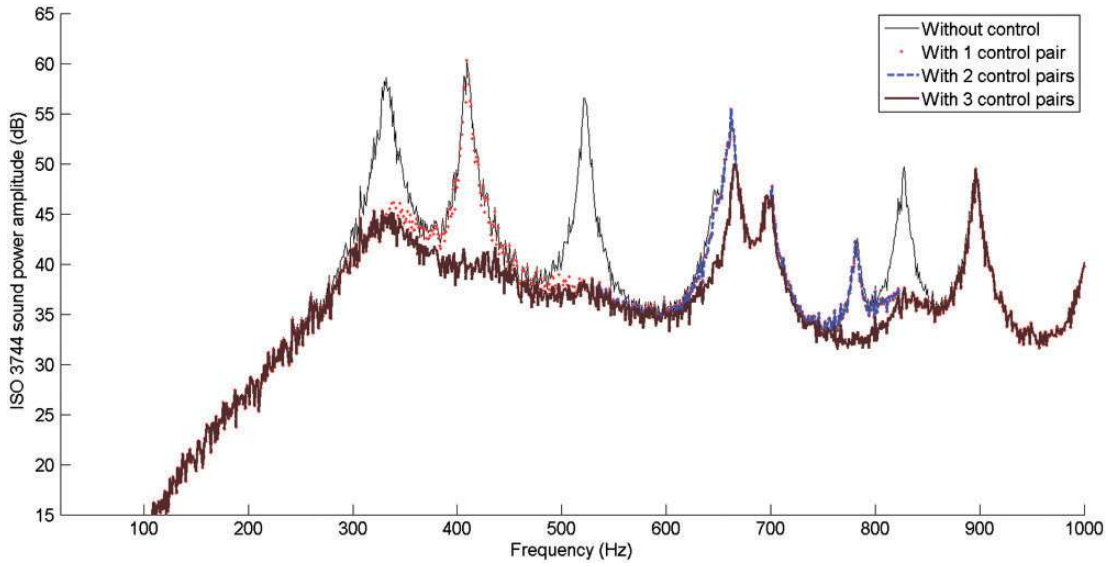

Figure 20. Control result of sound radiation power of the plate with different number of control pairs.

simulation results are the same as Figures 7 and 8 (tensioned case), since no active control acts on this band.

Remark: In this paper, idealized sensor/actuator arrangement is considered, thus the control system will not be influenced by the sensor/actuator dynamics, time delay caused by filter, digital controller etc. Accordingly, the control results bring an upper achievable noise reduction when using the proposed control law.

6. Conclusions

The turbulent boundary layer induced noise and vibration suppression with decentralized collocated velocity feedback control is investigated in this study. The semi-empirical TBL model selection is a combination model of Goody and Corcos.

The model scale of a finite element model is downsized in two steps. The first step transforms the N degrees of freedom into modal domain; the second uses sorted modal contribution to reduce model. When properly active damping is exerted on the plate, the final sound radiation control effect is largely determined by the number of sensor/actuator and their location.

Assuming the practical active control band is within 1 kHz, according to the structure sound radiation properties under TBL excitation, both the sound radiation efficient modes and the highly excited modes are needed to be controlled. Only controlling the volumetric modes are less effective for the sound radiation suppression, and more control channels are needed for decentralized feedback control.

For instance, when three channel control loops are used, nearly 5 dB sound radiation suppression is achieved in our study. Since the passive control is usually very effective above 1 kHz, it is anticipated that combining active control in low frequencies and passive control in the mid and high frequencies could achieve satisfying sound attenuation.

Finally, in the simulation case, determination of sensor/actuator location is simply based on the mode shapes, which may not be the optimal configuration. Therefore, advanced methods to optimize the sensor/actuator location could be used in the future. It will also be interesting to develop some optimal gain tuning law for collocated velocity feedback control, which can be utilized for actual experimental tests.

Acknowledgements

The authors would like to thank Professor MN Ichchou for his valuable suggestions. The authors sincerely thank the reviewers for their valuable comments and suggestions that have led to the present improved version.

Conflict of interest

The authors declare no conflict of interest.

Funding

This research is supported by National Natural Science Foundation of China (grant number 51375228), Aeronautical Science Fund (grant number 20131552025), China Postdoctoral Science special Foundation (grant number 2014T70514), the Fundamental Research Funds for

the Central Universities (grant number NJ20140012) and PAPD, China Scholarship Council and Funding of Jiangsu Innovation Program for Graduate Education (grant number CXLX11_0186).

References

Balas MJ (1979) Direct velocity feedback control of large space structures. *Journal of Guidance, Control, and Dynamics* 2: 252–253.

Bianchi E, Gardonio P and Elliott S (2004) Smart panel with multiple decentralized units for the control of sound transmission. Part III: control system implementation. *Journal of Sound and Vibration* 274: 215–232.

Blake WK (1986) *Mechanics of Flow-Induced Sound and Vibration*. London: Academic Press.

Chase D (1987) The character of the turbulent wall pressure spectrum at subconvective wavenumbers and a suggested comprehensive model. *Journal of Sound and Vibration* 112: 125–147.

Corcos G (1963) Resolution of pressure in turbulence. *J Acoust Soc Am* 35: 192–199.

De Rosa S and Franco F (2008) Exact and numerical responses of a plate under a turbulent boundary layer excitation. *Journal of Fluids and Structures* 24: 212–230.

Doyle JC, Francis BA and Tannenbaum A (1992) *Feedback control theory*. New York: Macmillan Publishing Company.

Efimtsov B (1982) Characteristics of the field of turbulent wall pressure fluctuations at large Reynolds numbers. *Soviet Physics Acoustics* 28: 289–292.

Efimtsov B and Lazarev L (2012) A complex of analytical models for predicting noise in an aircraft cabin. *Acoustical Physics* 58: 404–410.

Elliott SJ, Gardonio P, Sors TC, et al. (2002) Active vibroacoustic control with multiple local feedback loops. *J Acoust Soc Am* 111: 908–915.

Engels WP, Baumann ON, Elliott SJ, et al. (2006) Centralized and decentralized control of structural vibration and sound radiation. *The journal of the Acoustical Society of America* 119: 1487–1495.

Fuller CR, Elliott S and Nelson PA (1997) *Active control of vibration*. London: Academic Press.

Gardonio P (2002) Review of active techniques for aerospace vibro-acoustic control. *Journal of Aircraft* 39: 206–214.

Gardonio P (2013) Boundary layer noise–Part 2: Interior noise radiation and control. *Noise Sources in Turbulent Shear Flows: Fundamentals and Applications*. Berlin: Springer.

Gardonio P, Bianchi E and Elliott S (2004a) Smart panel with multiple decentralized units for the control of sound transmission. Part I: theoretical predictions. *Journal of Sound and Vibration* 274: 163–192.

Gardonio P, Bianchi E and Elliott S (2004b) Smart panel with multiple decentralized units for the control of sound transmission. Part II: design of the decentralized control units. *Journal of Sound and Vibration* 274: 193–213.

Gardonio P and Elliott SJ (2005a) Modal response of a beam with a sensor–actuator pair for the implementation of velocity feedback control. *Journal of Sound and Vibration* 284: 1–22.

Gardonio P and Elliott SJ (2005b) Smart panels with velocity feedback control systems using triangularly shaped strain actuators. *J Acoust Soc Am* 117: 2046–2064.

Gibbs G, Cabell RH and Juang J-N (2004) Controller complexity for active control of turbulent boundary-layer noise from panels. *AIAA Journal* 42: 1314–1320.

Goody M (2004) Empirical spectral model of surface pressure fluctuations. *AIAA journal* 42: 1788–1794.

Graham W (1996) Boundary layer induced noise in aircraft, Part I: The flat plate model. *Journal of Sound and Vibration* 192: 101–120.

Graham W (1997) A comparison of models for the wavenumber–frequency spectrum of turbulent boundary layer pressures. *Journal of Sound and Vibration* 206: 541–565.

Howe MS (1998) *Acoustics of fluid-structure interactions*. Cambridge: Cambridge University Press.

Hwang Y, Bonness WK and Hambric SA (2009) Comparison of semi-empirical models for turbulent boundary layer wall pressure spectra. *Journal of Sound and Vibration* 319: 199–217.

Ichchou M, Hiverniau B and Troclet B (2009) Equivalent 'rain on the roof'loads for random spatially correlated excitations in the mid–high frequency range. *Journal of Sound and Vibration* 322: 926–940.

Lesieur M (2005) *Large-eddy simulations of turbulence*. Cambridge: Cambridge University Press.

Liu B (2008) Noise radiation of aircraft panels subjected to boundary layer pressure fluctuations. *Journal of Sound and Vibration* 314: 693–711.

Liu B, Feng L, Nilsson A, et al. (2012) Predicted and measured plate velocities induced by turbulent boundary layers. *Journal of Sound and Vibration* 331: 5309–5325.

Maury C and Bravo T (2006) The experimental synthesis of random pressure fields: Practical feasibility. *J Acoust Soc Am* 120: 2712–2723.

Maury C, Gardonio P and Elliott S (2001) Active control of the flow-induced noise transmitted through a panel. *AIAA Journal* 39: 1860–1867.

Maury C, Gardonio P and Elliott S (2002) A wavenumber approach to modelling the response of a randomly excited panel, Part II: Application to aircraft panels excited by a turbulent boundary layer. *Journal of Sound and Vibration* 252: 115–139.

Meirovitch L (1990) *Dynamics and control of structures*. New York: Wiley.

Miller TS, Gallman JM and Moeller MJ (2012) Review of Turbulent Boundary Layer Models for Acoustic Analysis. *Journal of aircraft* 49: 1739–1754.

Ohayon R and Soize C (1998) *Structural acoustics and vibration: Mechanical models, variational formulations and discretization*. London: Academic Press.

Ohayon R and Soize C (2014) *Advanced computational vibroacoustics*. Cambridge: Cambridge University Press.

Preumont A (2011) *Vibration control of active structures: an introduction*. Berlin: Springer.

Rocha J and Palumbo D (2012) On the sensitivity of sound power radiated by aircraft panels to turbulent boundary

layer parameters. *Journal of Sound and Vibration* 331: 4785–4806.

Rohlfing J and Gardonio P (2009) Homogeneous and sandwich active panels under deterministic and stochastic excitation. *J Acoust Soc Am* 125: 3696–3706.

Rohlfing J and Gardonio P (2014) Ventilation duct with concurrent acoustic feed-forward and decentralised structural feedback active control. *Journal of Sound and Vibration* 333: 630–645.

Schiller NH, Cabell RH and Fuller CR (2010) Decentralized control of sound radiation using iterative loop recovery. *J Acoust Soc Am* 128: 1729–1737.

Schiller NH, Perey DF and Cabell RH (2011) *Development of a Practical Broadband Active Vibration Control System*. ASME 2011 International Mechanical Engineering Congress & Exposition. Denver, Colorado, USA: ASME, pp. 1–8.

Schlichting H and Gersten K (2000) *Boundary-layer theory*. Berlin: Springer.

Skogestad S and Postlethwaite I (1996) *Multivariable feedback control: analysis and design*. New York: Wiley-Interscience.

Wallace C (1972) Radiation resistance of a rectangular panel. *J Acoust Soc Am* 51: 946–952.

Wang Y and Inman DJ (2011) Comparison of control laws for vibration suppression based on energy consumption. *Journal of Intelligent Material Systems and Structures* 22: 795–809.

Wilby J (1996) Aircraft interior noise. *Journal of Sound and Vibration* 190: 545–564.

Yuan M, Ji H, Qiu J, et al. (2012) Active control of sound transmission through a stiffened panel using a hybrid control strategy. *Journal of Intelligent Material Systems and Structures* 23: 791–803.

Yuan M, Qiu J, Ji H, et al. (2013) Active control of sound transmission using a hybrid/blind decentralized control approach. *Journal of Vibration and Control*. Epub ahead of print December 19, 2013, doi: 10.1177/1077546313514758.

Zhang K, Scorletti G, Ichchou M, et al. (2013) Phase and gain control policies for robust active vibration control of flexible structures. *Smart Materials and Structures* 22: 1–15.

Zhang K, Scorletti G, Ichchou MN, et al. (2014) Robust active vibration control of piezoelectric flexible structures using deterministic and probabilistic analysis. *Journal of Intelligent Material Systems and Structures* 25: 665–679.